

# Reconstruction of neuromorphic dynamics from a single scalar time series using variational autoencoder and neural network map

Pavel V. Kuptsov<sup>1, a)</sup> and Nataliya V. Stankevich<sup>1, b)</sup>

*Laboratory of topological methods in dynamics, HSE University, 25/12 Bolshaya Pecherskaya str., Nizhny Novgorod 603155, Russia*

(Dated: 12 November 2024)

This paper examines the reconstruction of a family of dynamical systems with neuromorphic behavior using a single scalar time series. A model of a physiological neuron based on the Hodgkin-Huxley formalism is considered. Single time series of one of its variables is shown to be enough to train a neural network that can operate as a discrete time dynamical system with one control parameter. The neural network system is created in two steps. First, the delay-coordinate embedding vectors are constructed from the original time series and their dimension is reduced with by means of a variational autoencoder to obtain the recovered state-space vectors. It is shown that an appropriate reduced dimension can be determined by analyzing the autoencoder training process. Second, pairs of the recovered state-space vectors at consecutive time steps supplied with a constant value playing the role of a control parameter are used to train another neural network to make it operate as a recurrent map. The regimes of thus created neural network system observed when its control parameter is varied are in very good accordance with those of the original system, though they were not explicitly presented during training.

One of the most appealing characteristics of neural networks is their ability for data generalization. This is achieved through the extraction of data features and dependencies that may initially appear obscure. In the context of dynamical systems reconstruction, this aptitude could facilitate significant advancements in the development of models based on experimental data. In this paper, we investigate the extent to which neural networks can reproduce the dynamical regimes of a system, observed for various values of its control parameters, when only a single scalar time series of this system is available. Created neural network models a family of dynamical systems parameterized by a control parameter. This family exhibits behavior consistent with that of the original system, i.e. discovers its specific regimes and transitions. This is demonstrated by the example of a neuromorphic Hodgkin-Huxley system. The reconstruction is carried out in two steps. Initially, a variational autoencoder is trained to convert the time series into a sequence of reconstructed state vectors. These are then used for training a neural network map. The trained map operates as a dynamical system with discrete time, having one control parameter. We show

that it is capable of reproducing the dynamical regimes of the original system, including those that were not demonstrated during training.

## I. INTRODUCTION

Reconstructing dynamical models from time series is an important task from a practical point of view and also is an interesting theoretical challenge. To date, a large number of approaches and methods for solving this problem have been developed<sup>1-3</sup>. In connection with the intensive development of artificial neural network technologies, it seems interesting to study their capabilities in relation to the dynamical modeling. In this regard, without claiming completeness, we can mention some related works. In papers<sup>4-6</sup> a sort of neural networks techniques called reservoir computing is considered as tool for replicating the dynamics of chaotic systems and predicting their properties. Blending several dynamical systems into a single model built on the bases of reservoir computing is considered in papers<sup>7,8</sup>. In paper<sup>9</sup> recurrent neural network is considered as a tool for reconstruction of a model of dynamics trained directly on the measured physiological data. Paper<sup>10</sup> reports a new framework, Gumbel Graph Network, which is a model-free, data-driven deep learning framework to accomplish the reconstruction of both network connections and the dynamics on it. Paper<sup>11</sup> is devoted to reconstruction of chaotic dynamic from scalar time series using plain autoencoder.

Along with the reconstruction of dynamical systems, neural networks and machine learning methods inspire new ideas in other fields of nonlinear dynamics. In particular, a series of papers<sup>12-14</sup> develops a technique of

<sup>a)</sup>Electronic mail: kupav@mail.ru, corresponding author; also at Kotelnikov Institute of Radio-Engineering and Electronics of Russian Academy of Sciences, Saratov Branch, 38 Zelenaya str., Saratov 410019, Russia

<sup>b)</sup>Electronic mail: stankevichnv@mail.ru; also at Kotelnikov Institute of Radio-Engineering and Electronics of Russian Academy of Sciences, Saratov Branch, 38 Zelenaya str., Saratov 410019, Russia

dynamical learning of synchronization (DLS) designed to control the synchronization state of a complex network composed of nonlinear oscillators. Paper<sup>15</sup> demonstrates that a three-layer neural network, comprising input, training, and output layers and utilizing spike-timing-dependent plasticity (STDP), can effectively learn the orderly propagation of signals between network layers under controlled synaptic conditions. Neural networks are used for adaptive modeling and control of dynamical systems<sup>16</sup>, applied for El Niño attractor reconstruction<sup>17</sup>, employed for dynamics prediction based on state space reconstruction<sup>18</sup>. Also machine learning is utilized for biological models creations and analysis<sup>19</sup>.

One of the most appealing characteristics of neural networks is their capacity for data generalization. This ability stems from the fact that a well-trained neural network is able to identify and extract from the data features and dependencies that may initially appear to be obscure. In the context of problems related to dynamics reconstruction, this aptitude should facilitate significant advancements in the direction of developing models based on experimental data. It is natural to expect that even with a limited amount of information about the system, such as its single scalar time series, it will be possible to use a neural network to construct a family of models, parameterized by control parameters, that will be able to predict a variety of system behaviors.

Our paper considers this possibility in relation to a specific example: the neuromorphic dynamics of a system built on the basis of the Hodgkin-Huxley formalism. We avoid using simplified neuron models and focus on the realistic Hodgkin-Huxley one since planing in our future works to consider an experimental data obtained from a natural system described within the Hodgkin-Huxley framework.

The main motivation of this paper is to contribute to the methods of studying dynamics based on experimental data. However, in this paper we define a modeled system using ODEs and get a time series from numerical solving the equations. It means that our data are devoid of the features inherent in the data of a real experiment: they are sampled with a small and constant time step, there are quite a lot of them, the readings are recorded without errors (except for numerical ones) and they are not noisy. The cases with non-perfect experimental data will be considered in our subsequent studies.

We use variational autoencoder (VAE)<sup>20,21</sup> and neural network map<sup>22,23</sup> as tools to perform reconstruction. The VAE is used to recover system state vectors by reducing the dimension of delay-coordinate embedding vectors from the original time series. The recovered state-space vectors are then used to train the neural network map, resulting in a reconstructed dynamical system with a single control parameter.

An autoencoder is one of the standard neural network architectures, which is used, among other things, to reduce the dimension of data<sup>21</sup>. The main feature of an autoencoder is that the data vectors it process at some

point passes through a bottleneck, that is, it turns out to be represented in the form of low-dimensional vectors. The first part of the autoencoder, called the encoder, is responsible for this. After this, the dimension is restored to the original value by the second part, called the decoder. The objective of training is to achieve a minimal discrepancy between the input and output vectors. To this end, all pertinent data must be compressed into the reduced vectors at the bottleneck.

VAE differs from a plain autoencoder in that the output of the encoder is not the reduced vector itself, but parameters of the so-called latent space. The reduced vector is randomly selected from this latent space and passed to the decoder. Random sampling of the reduced vectors from the latent space during training is very important for the purposes of dynamics reconstruction, as it ensures proximity preservation. Thanks to this, it is guaranteed that fragments of the original trajectory that are close to each other will be represented by the close latent space vectors, which we use as the reconstructed state-space vectors of the modeled system.

It is mathematically proven<sup>24-29</sup> that a two-layer fully connected, i.e., dense, neural network can be used to approximate arbitrary functions of many variables. It means that it can be suitable for reconstruction of a dynamical system. In paper<sup>30</sup> a good quality of dynamics reproduction with such a simple network model was shown for different systems: Lorenz, Rössler, Hindmarch-Rose neuron model. However, already for the Hindmarch-Rose oscillator the quality of reconstruction was lower than for two other systems. It was found that a neural network map based on a simple two-layer structure is difficult to train for so called stiff systems where variables have very different time scales. Then in paper<sup>22</sup> a more advanced structure of the neural network map was suggested. Instead of a single network accepting the full state vector at once and returning the state vector on the next time step, subnetworks for each dynamical variable were introduced. Each subnetwork still has two-layer structure, but all other variables together with control parameters are injected after an additional dense layer. Such network is found to model stiff dynamics and also is able to discover correctly dynamical regime not shown during training. In paper<sup>23</sup> it is shown that two neural network maps trained separately can model dynamics of two coupled systems without additional training.

Thus the goal of this study is to reconstruct the dynamics of a system as completely as possible, given its single scalar time series, using neural networks. The result of the reconstruction will be a family of dynamical systems, parameterized by a control parameter. Our particular interest will be in the dynamical features of the modeled system that are not explicitly presented during training and nevertheless discovered by the reconstructed system.

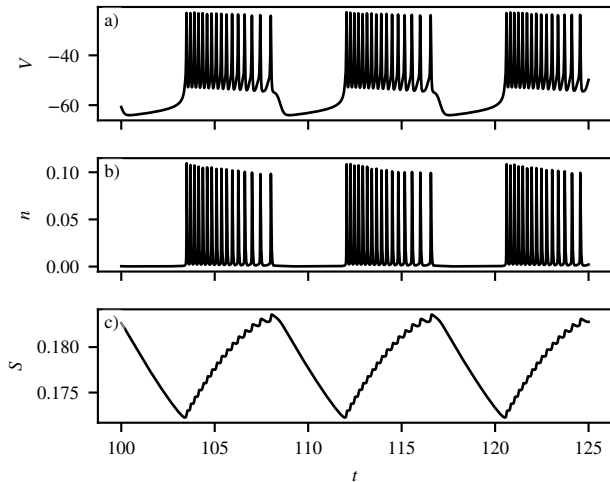


FIG. 1. Solution of the system (1) in the regime of bursting oscillations.  $k = 0$  and  $V_S = -36$ . Other parameters see in Tab. I.

## II. HODGKIN-HUXLEY-TYPE MODEL

We consider a model of a physiological neuron based on the Hodgkin-Huxley formalism<sup>31</sup>, and also modification<sup>32</sup> that is responsible for bistability in a certain parameter range when bursting oscillations coexist with a stable equilibrium point,

$$\begin{aligned}\tau\dot{V} &= -I_{Ca}(V) - I_K(V, n) - I_S(V, S) - kI_{K2}(V), \\ \tau\dot{n} &= \sigma[n_\infty(V) - n], \\ \tau_S\dot{S} &= S_\infty(V) - S.\end{aligned}\quad (1)$$

Here  $V$ ,  $n$  and  $S$  are dynamical variables. In the considered parameter ranges the system (1) has a single unstable fixed point. The modification resulting in its stabilization is introduced via the function  $I_{K2}(V)$ . It will be switched on and off by the coefficient  $k \in \{0, 1\}$ . We will consider the system (1) for varying  $V_S$  at  $k = 0$  (the original system) and  $k = 1$  (the modified system). All other numerical values of parameters as well as the functions included in these equations are given in Appendix A, see Table I and Eqs. (A1).

System (1) is stiff since it has one slow and two fast variables with very different rates of oscillations. Effective numerical solution of a system like this is possible with specially designed methods. We will use a stiff solver implementing Radau method<sup>33</sup>.

Dynamics of the system (1) at  $k = 0$  is illustrated in Figs. 1 and 2. Figure 1 represents bursting oscillations at  $V_S = -36$ . Observe that  $V$  and  $n$  oscillate fast while  $S$  is a slow variable. When  $V_S$  gets larger spiking regime emerges as shown in Fig. 2 that is plotted at  $V_S = -33$ . Solutions of the modified system at  $k = 1$  are not shown since they are visually indistinguishable from those in Figs. 1 and 2.

Figure 3 shows how dynamics of the system (1) at

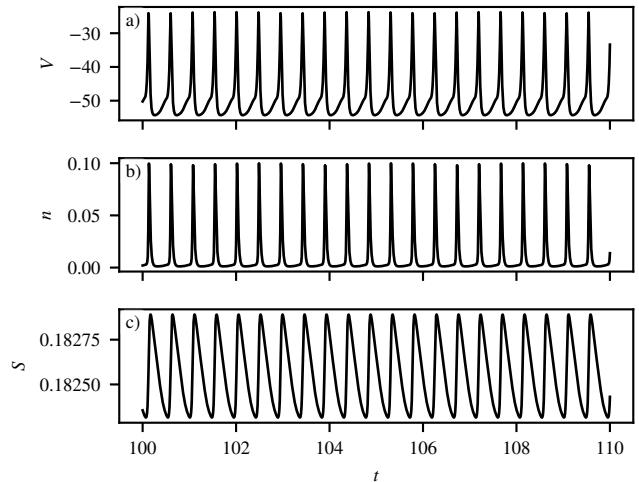


FIG. 2. Spiking of the system (1) at  $k = 0$  and  $V_S = -33$ ; also see Tab. I.

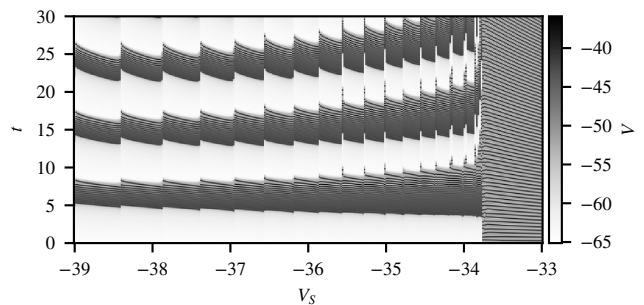


FIG. 3. Diagram of regimes of the system (1) at  $k = 0$ . The horizontal axis shows the change in parameter  $V_S$ . For each  $V_S$  a solution of the system (1) is computed and values of  $V(t)$  are shown along the vertical axis with gray shapes. The darker shades indicate higher values. The plotted solutions are recorded after omitting transients and are aligned by the smallest minimum on the curve  $V(t)$ .

$k = 0$  changes. Here  $V_S$  varies along the horizontal axis, time goes vertically and shades of gray indicate values of dynamical variable  $V$  recorded after omitting transients and aligned by the smallest minimum on the curve  $V$ . Burst in the left part of the figure looks like three stripes that vanish at  $V_S \approx -33.73$  due to the bifurcation transition associated with a blue-sky catastrophe<sup>32,34</sup>. To the right of this point high frequency spiking oscillations appear that are represented in the diagram as a uniform texture.

Bistability at  $k = 1$  is shown in Fig. 4. For  $V_S$  approximately between  $V_S = -37$  and  $V_S = -35$  there is a stable fixed point. At  $V_S = -36$  the fixed point is  $V = -50.636$ ,  $n = 2.0560 \times 10^{-3}$ ,  $S = 0.18792$ , and its stability is indicated by the negative eigenvalues  $(-0.15927, -19.521, -38.785)$ . The stable fixed point coexists with the bursting oscillations. To draw Fig. 4 we begin at  $V_S = -36$  and continue the solution step by step first to the left

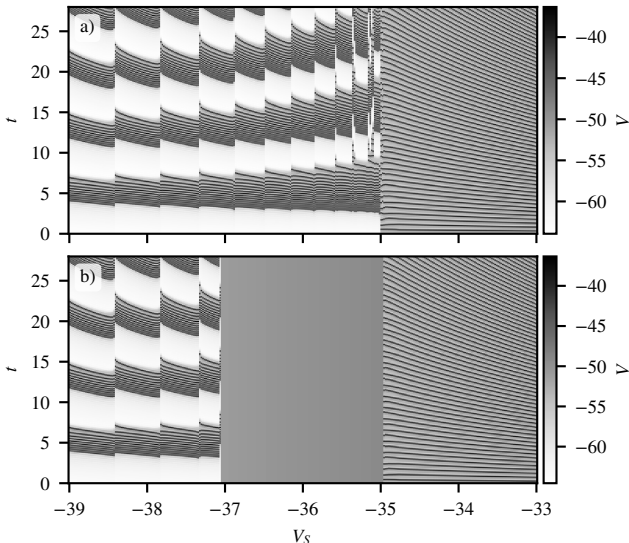


FIG. 4. Diagram of regimes of the system (1) at  $k = 1$ . Panels (a) and (b) illustrate the bistability. To plot each panel we compute one of two coexisting solutions in the middle of the plot at  $V_S = -36$ : (a) the bursts and (b) the fixed point. Then this solution is continued to the left and to the right, i.e., computation at new parameter step starts from the last point obtained at the previous step

and to then the right of this parameter value always taking the last trajectory point at the previous parameter step as the initial point for the next parameter step. In Fig. 4(a) the very starting point for the trajectory at  $V_S = -36$  arrives after a transient at the bursting oscillations. Doing continuation of this solution we observe a picture that is very similar to the system at  $k = 0$ , cf. Fig. 3. And when the very starting point is taken near the stable fixed point, as in Fig. 4(b), the flat area appears in the figure that represents the staying the system at the fixed point.

### III. RECONSTRUCTION STATE-SPACE VECTORS USING VARIATIONAL AUTOENCODER

#### A. Approach in general

Autoencoders are neural networks that are trained via self supervised procedure<sup>20,21</sup>. The training vectors  $R$  are forwarded to the network and the goal of the training is to restore at the output the vectors  $R'$  as close as possible to  $R$ . The loss function of the training is the distance between  $R$  and  $R'$ . The key point is the presence of a bottleneck. The autoencoder consists of two parts, an encoder and a decoder. The encoder maps the input vectors  $R$  to the space of reduced vectors  $u$  of smaller dimension, and the decoder maps them back to the original space of  $R$ . Due to the squeezing the data through the low dimensional space, the network is forced to ex-

tract the most essential data features sufficient for their further restoring.

In plain autoencoders the encoder output  $u$  goes directly to the decoder input. VAE encoder generates parameters of so called latent space, usually they are a mean value  $\mu$  and a standard deviation  $\sigma$  of a Gaussian distribution. The decoder input vector  $u$  is a random sample from this distribution. The mathematics theory of VAEs can be found in paper<sup>20</sup> and for the software implementation we have followed the description from the book<sup>21</sup>.

We will use VAEs for state-space vector reconstruction. At first glance, random sampling from the latent space introduces unnecessary stochasticity to reconstruction procedure. Plain autoencoders that do not use the random sampling can also be used for dimension reduction of phase space vectors<sup>11,35</sup>. However, plain autoencoders do not guarantee a continuity of the space of the reduced vectors. Close input vector will not necessarily be mapped to the close vectors in the latent space merely since no limitation is applied to the training process that would force this property to appear. For the dynamic reconstruction it means that given close parts of the modeled trajectory there are no reasons to expect that the encoder will always map them to close reconstructed state-space vectors. The proximity preservation in the latent space is very important since without it the reconstructed system will be inappropriate for method of stability analysis based on small perturbations, like computation of Lyapunov exponents. It is the random sampling from the latent space that provides the very training constraint that ensures the proximity preservation<sup>20</sup>. Thanks to it, not only the exact vector  $u = \mu$  will be mapped back to  $R' \approx R$  but also its small perturbations will also be mapped to vectors close to  $R$ . Proximity preservation can be treated as a sort of robustness: two similar system will obtain similar models, and a small neighborhood of the original trajectory will be mapped to a small neighborhood of the trajectory of the reconstructed system.

Consider a dynamical system given by ODEs:

$$\dot{U} = f(U), \quad (2)$$

where  $U = U(t)$  is a state-space vector of dimension  $D_u$ . This equation is solved numerically to obtain a discrete time series of vectors with constant time step  $\Delta t$ . Then only one scalar component  $U_i(n) = U_i(t_0 + n\Delta t)$ ,  $i \in \{1, 2, \dots, D_u\}$ , is taken for further processing. The choice of  $i$  is a subject of a separate discussion.

This step models an experimental situation when the full vector as well as an underlying dynamical system are unknown and the only scalar time series is available. In this paper we do not consider a realistic situation when the data record is written with noises, with large discretization step and is too short. We just take “good” numerical data and left more realistic cases for further studies.

The standard first step of data preparation is the rescaling of  $U_i(n)$  to fit the range  $[-1, 1]$  for the neural

network training algorithm to work properly. Then this data series is transformed to delay-coordinate embedding vectors<sup>36,37</sup>  $R(n)$  of dimension  $D_e$ :

$$R(n) = (U_i(n), U_i(n-1), \dots, U_i(n-D_e+1)). \quad (3)$$

The dimension  $D_e$  is usually unknown in model reconstruction procedure. There are rather heuristic algorithms of their determinations<sup>1,37</sup>. We will not use them since dimension reduction procedure via VAE is not sensible to the very exact choice of  $D_e$ . It is enough to take it excessively large.

Vectors  $R$  are used to train the VAE whose detailed structure is described in Appendix B. The result is a two-step map. The first part, the encoder, maps  $R$  to two vectors  $\mu$  and  $\sigma$  of the reduced dimension  $D_u$ . The second part, the decoder, maps a random sample  $u$  of a Gaussian distribution  $N(\mu, \sigma)$  to a vector  $R'$  that is approximately equals to  $R$ .

## B. Variational autoencoder for the Hodgkin-Huxley-type model

We are going to model the periodic bursting oscillations of the system (1), like those shown in Fig. 1. The information about the modeled system is limited by a single period. The period size depends on the parameters and approximately equals to  $T \approx 10$ . Step size of time discretization is  $\Delta t = 0.005$ . The scalar time series of one period length is sliced into the delay-coordinate embedding vectors  $R(n)$  of dimension  $D_e = 32$ , see Eq. (3).

The approach we develop is not sensible to the particular choice of  $D_e$  provided that it excessively larger then dimension of the considered system  $D_u = 3$ . This is the advantage of using VAE for state vector recovery. However to make sure we checked various  $D_e$ : 16, 32, 64, 128 and 512, and all worked equally well.

The approximate size of the resulting dataset is  $T/\Delta t \approx 2000$  which is small. Training a neural network on a small dataset usually results in the network simply memorising the data instead of the desired generalization of the data, i.e. the extraction of their essential features. One of the standard methods to improve this situation is data augmentation. We perform it as follows: the trajectory cut of one period length is supplied with its 19 copies perturbed by a small Gaussian noise with zero mean and the standard deviation  $1/200$ . Besides the improved data generalization the augmentation serves for better robustness: the obtained VAE is trained to encode and decode not the unique trajectory, but a small cloud of them.

The result of the VAE training is found to depend on the choice of the scalar variable for reconstruction. Figure 5 shows that integration of the fast variables  $V$  and  $n$  of the system (1) results in slow curves that look very similar to  $S$ . The differentiating of  $S$  produces the bursting curve whose shape is very similar to  $V$ . As already discussed above a scalar time series is converted to delay-coordinate embedding vectors  $R(n)$  of the dimension  $D_e$ .

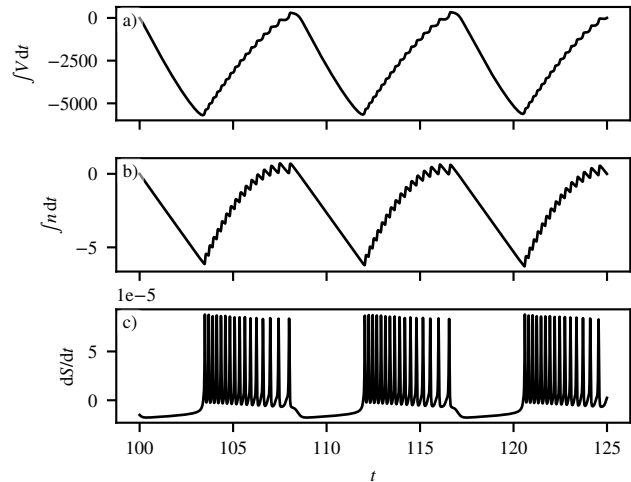


FIG. 5. Integrated  $V(t)$  and  $n(t)$ , panels (a) and (b), respectively, and differentiated  $S(t)$ , panel (c), taken from Fig. 1.

The network processes each of these vectors separately so that it can operate only with trajectory pieces of the length  $D_e$ . It means that VAE cannot integrate the whole input time series to find a slow variable given a fast one. But it can differentiate data since this is a local operation so that all necessary information is available for it. Moreover, the convolution layer employed in the encoder, see Fig. 15(b), can perform the differentiation provided that its weights are tuned properly.

As a result when  $S$  is used for training VAE, its encoder is able to reconstruct two fast and one slow variable and being trained for  $V$  or  $n$  it cannot reconstruct a slow variable. This is shown in Fig. 6. Panels (a-c) demonstrate initial data obtained as a solution of Eqs. (1) at  $V_s = -36$  and  $k = 0$  on a single period  $T = 9$  with the time step  $\Delta t = 0.005$ . Panels (d-f) show vectors  $u(n) = \mu(n)$  obtained at the VAE encoder output that is forwarded by the embedding vectors obtained for  $S$ . Observe a very good correspondence of  $V$  and  $u_1$  and also  $S$  and  $u_3$ . As for  $n$  its reconstructed version  $u_2$  demonstrates similar burst and the only difference is that  $u_2$  oscillates up and down with respect to the middle level while for  $n$  there is a minimum level and bursts occur only above it. Nevertheless VAE encoder performance is good as a whole: panels (a-c) and their reconstruction are qualitatively similar to each other. Notice that the variables  $u_1$ ,  $u_2$  and  $u_3$  appears in an arbitrary order. We reorder them manually to fit the sequence  $V$ ,  $n$  and  $S$  of the system (5). Quite different result is obtained for VAE trained on  $V$ , see panels (g-i). Variables  $V$  and  $n$  correspond to the reconstructed variables  $u_1$  and  $u_2$ , but no slow variable similar to  $S$  appears. Instead  $u_3$  demonstrate bursts rather similar to  $u_2$ . Thus in what follows we will take time series of  $S(n)$  to create a reconstructed system.

When a dynamical system is represented by its scalar time series the true value of the dimension  $D_u$  is unavail-

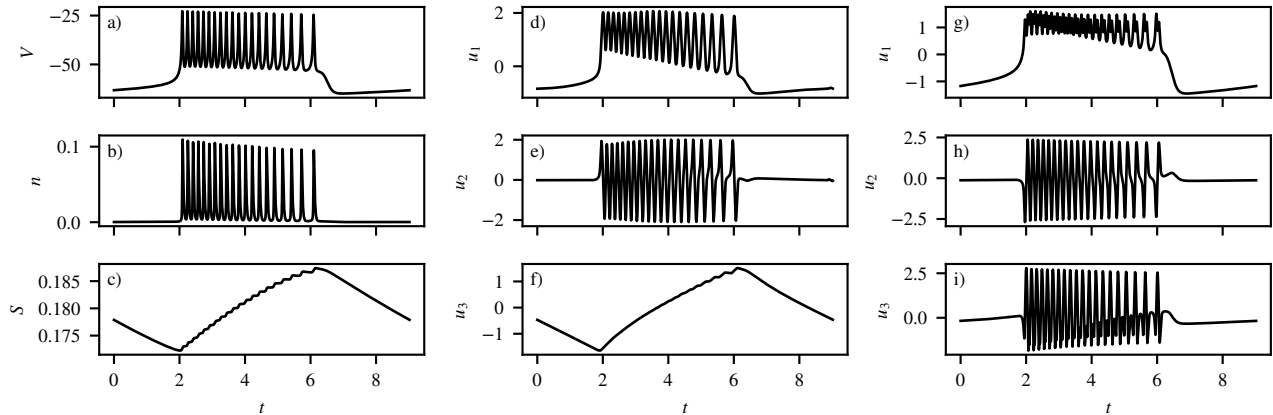


FIG. 6. Panels (a), (b) and (c) depict one period of a bursting trajectory of the system (1) at  $V_S = -36$  and  $k = 0$ . Panels (d), (e) and (f) illustrate output of the VAE encoder trained on the time series for  $S(t)$  from the panel (c). Panel (g), (h) and (i) — output of the VAE encoder trained on  $V(t)$  from the panel (a).

able. When performing state vector reconstruction using a plain autoencoder, one way to determine it is to impose an additional constraint on the vectors in the latent space by requiring that their sparsity to be maximised during training. This method is used in paper<sup>11</sup>. We do not employ this approach since we consider a variational autoencoder. Its encoding part has two outputs  $\mu$  and  $\nu$  that are already constrained by the minimization of the Kullback–Leibler divergence, see Eq. (B1) and the paper<sup>20</sup> for corresponding theoretical considerations. Adding more constrains to  $\mu$  and  $\nu$  would require a modification of the mathematical foundation of variational autoencoders. Due to this reason we will merely build VAEs for different latent space dimension  $D_u$  and discuss how the guess of  $D_u$  influences the result of the reconstruction.

Figure 7 shows VAE encoder outputs computed for the same input data: one period of the variable  $S$  of the system (1) at  $V_S = -36$  and  $k = 0$ , see Fig. 6(c). VAEs are trained for six guesses of the dimension  $D_u = 1, 2, \dots, 6$ , moreover, for each  $D_u$  the training is performed two times starting from random initial weights  $w_e$  and  $w_d$  of the network. Totally the results of twelve VAEs are shown.

First of all notice that the components  $S$  that is used as training data is reconstructed correctly for all guesses of  $D_u$  and for all runs of training, see Figs. 7(a<sub>1</sub>, b<sub>1</sub>, . . . , f<sub>1</sub>).

When the dimension guess is enough for the second component to appear,  $D_u \geq 2$ , VAE encoders start to reconstruct the variable  $V$ , see Figs. 7(b<sub>2</sub>, c<sub>2</sub>, . . . , f<sub>2</sub>). Similarly when  $D_u \geq 3$  the component corresponding to  $n$  is recovered, Figs. 7(c<sub>3</sub>, d<sub>3</sub>, . . . , f<sub>3</sub>). Notice that when  $D_u \leq 4$  the recovering of “true” components of the system (1)  $S$ ,  $V$  and  $n$  is stable: curves for different runs of training are almost identical, compare solid and dashed curves in Figs. 7(a<sub>1</sub>, b<sub>1,2</sub>, c<sub>1,2,3</sub> and d<sub>1,2,3</sub>). When  $D_u = 5$  or 6, the different runs of the training results in not com-

pletely identical curves for  $V$  and  $n$ . Nevertheless they are still very similar, compare solid and dashed curves in Figs. 7(e<sub>2,3</sub> and f<sub>2</sub>). Summarizing, VAE firmly reproduces “true” components of the modeled system regardless of dimension  $D_u$  guess. However when  $D_u$  gets higher the reproduction accuracy deteriorates. When the guess for  $D_u$  is higher then the true one, spurious components appear. Analyzing the corresponding curves in Figs. 7(d<sub>4</sub>), 7(e<sub>4,5</sub>) and 7(f<sub>4,5,6</sub>) one sees that their shapes are unstable, i.e., they are different for different training runs, they are not reproduced with increasing  $D_u$  and one cannot find a pattern of their emerging.

Influence of the guess for  $D_u$  on VAEs performance is show in Fig. 8 that demonstrates dependence of mean absolute reconstruction error (MAE)  $\langle |R - R'| \rangle_{D_e}$  on the epoch of training. When the guess grow,  $D_u = 1, 2, 3$ , the error becomes smaller. One clearly see that  $D_u = 1$  and 2 are not enough for correct model reconstruction due to high error. But when  $D_u$  goes beyond the true value  $D_u = 3$  no further decrease of the error observed. Thus the increase of the latent space dimension improves VAE performance only until the dimension is less then the true one.

Therefore, the observations represented in Figs. 7 and 8 demonstrate that given a scalar time series VAEs are able to find the true dimension of an underlying dynamics.

## IV. NEURAL NETWORK MAP

### A. Structure of the neural network map

Assume that there is a time series  $u(n)$  of state-space vectors of a dynamical system sampled at time moments  $t_0 + n\Delta t$ , where  $\Delta t$  is a step of time discretization. We want to create a model for this dynamical system and for this purpose we find a function  $F(\cdot)$  that maps  $u(n)$  to

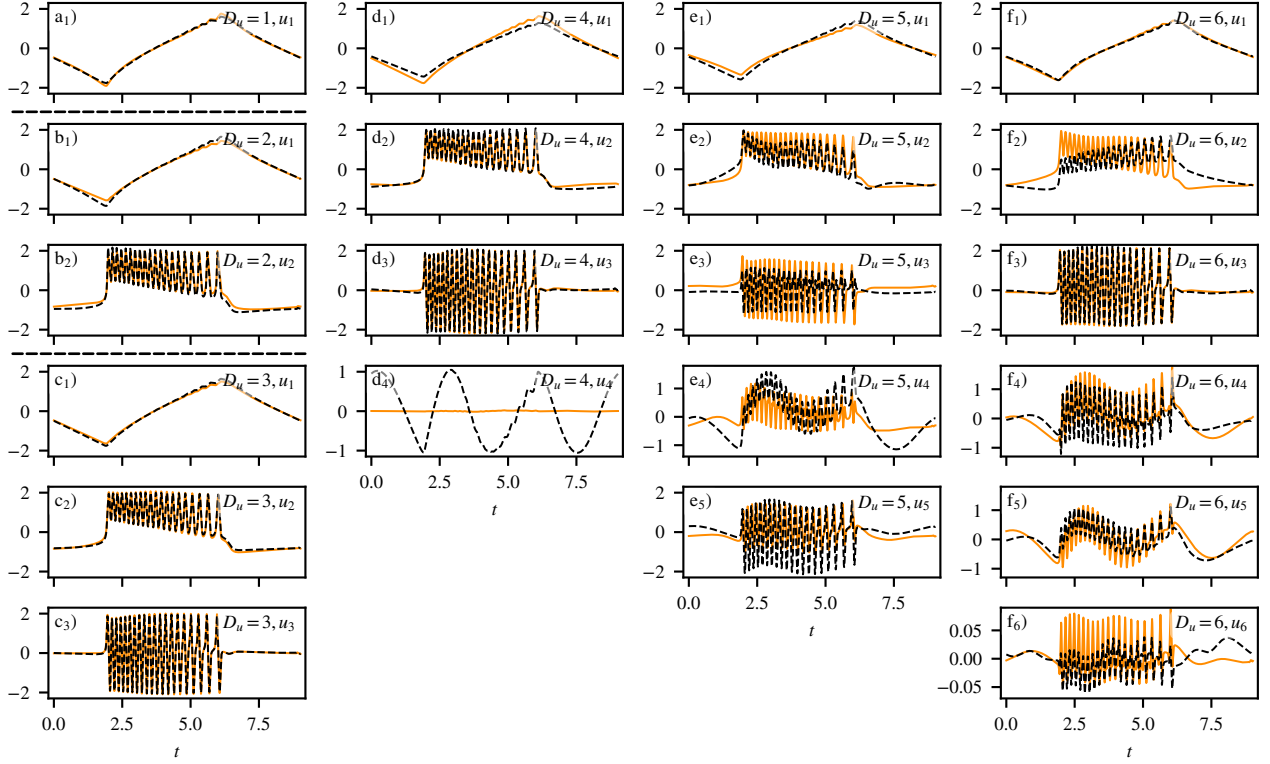


FIG. 7. Time series of the reconstructed state-space vectors  $u_i$  ( $i = 1, 2, \dots, D_u$ ), i.e., VAE encoder outputs, obtained when VAE is trained on the same time series  $S(t)$  at various  $D_u$ : (a<sub>1</sub>)  $D_u = 1$ ; (b<sub>1</sub>) and (b<sub>2</sub>)  $D_u = 2$ ; (c<sub>1</sub>)–(c<sub>3</sub>)  $D_u = 3$ ; (d<sub>1</sub>)–(d<sub>4</sub>)  $D_u = 4$ ; (e<sub>1</sub>)–(e<sub>5</sub>)  $D_u = 5$ ; (f<sub>1</sub>)–(f<sub>6</sub>)  $D_u = 6$ . The dashed horizontal lines between axis separate panels in the left column with different values of  $D_u$ . The training time series  $S(t)$  is shown in Fig. 6(c). Solid orange and dashed black curves on each panel illustrate two runs of VAE training with identical parameters and random initial weights. The curves for each VAE have been manually reordered to achieve correspondence between the curves for different  $D_u$ .

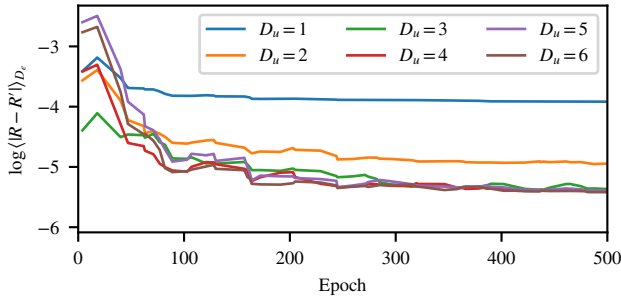


FIG. 8. Logarithms of mean absolute reconstruction error  $\langle |R - R'| \rangle_{D_e}$  as a function of epoch of training for six VAEs trained for various  $D_u$ .

$u(n+1)$ :

$$u(n+1) = F(u(n), p, w_m), \quad (4)$$

Here  $w_m$  is a vector of parameters that have to be tuned to adopt the recurrent map (4) for the desired behavior. Vector  $p$  collects control parameters of the dynamical system (4) introduced to model not only the precise time series  $u(n)$  but also regimes when parameters are varied.

We will create the map (4) as a neural network that operates according to the explicit formula<sup>22,23</sup>:

$$u_i(n+1) = u_i(n) + \chi \left( f \left( u_i(n) a_i + \mu_i + g(u_{-i}(n) A_i + p B_i + \beta_i) \right) b_i + \gamma_i \right). \quad (5)$$

This equation is build of scalars, vectors and matrices that are described in Tab. III in Appendix C. Vector of dynamical variables  $u(n)$  has dimension  $D_u$ . Scalar  $u_i(n)$  denotes its  $i$ th component and represents a dynamical variable of the  $i$ th subsystem. Vector  $u_{-i}(n)$  is obtained from  $u(n)$  by removing the  $i$ th component and thus has dimension  $D_u - 1$ . As usual for neural networks notation  $u(n)$  and  $u_{-i}(n)$  are treated as row-vectors. Control parameters are collected as a  $D_p$ -dimensional row-vector  $p$ . Functions  $f(\cdot)$  and  $g(\cdot)$  are called activation functions. They are scalar functions of scalar arguments and when they are applied to vectors, elements-wise operation is assumed.

Coefficient  $\chi$  is a small constant. It is required to stabilize the dynamics of the map (5). Without it the map even after a successful training can sometimes demonstrate the divergence. This is because the neural network

map (5) has a structure of the Euler scheme of numerical ODE solving with  $\chi$  playing the role of a time step. This scheme is known to diverges if the time step is too large<sup>38</sup>. Thus, the search for a suitable value of  $\chi$  reduces to finding the maximum time step at which the corresponding Euler scheme for Eq. (1) remains stable. Straightforward check revealed that the condition  $\chi < 0.01$  is enough for the stability, and thus for further computations we set  $\chi = \Delta t = 0.005$ .

Detailed description of the neural network map as well as discussion of its software implementation can be found in Appendix C.

### B. Neural network map for the reconstructed space-state vectors of the Hodgkin-Huxley-type model

To prepare the training data for the neural network map (5) we again take the embedding vectors  $R(n)$ , see Eq. (3) and forward them, now without the augmentation, to the VAE encoder. Its output is used to prepare a time series of reconstructed state-space vectors  $u(n)$ . These vectors are element-wise scaled to fit the range  $[-1, 1]$  for standard neural network training algorithms to work properly. Sequence of the resulting vectors correspond to time steps  $\Delta t$  of the original system (1).

To prepare the dataset for training the neural network map (5), we use the VAE encoder output  $\mu(n)$  and  $\sigma(n)$  in two ways. First, each  $u(n)$  is sampled from a random distribution parameterized by  $\mu(n)$  and  $\sigma(n)$ . Second, we set directly  $u_\mu(n) = \mu(n)$ , shift it by one step, and compose pairs  $(u(n), u_\mu(n+1))$ . Here  $u(n)$  will be forwarded to the input of the trained network and  $u_\mu(n+1)$  will be its desired output. The full dataset includes 20 repetitions of this procedure for the whole set of the embedding vectors  $R(n)$ , so that there are 20 slightly different sets of  $u(n)$  each corresponding to the same  $u_\mu(n+1)$ . The loss function is mean squared error  $(u'(n+1) - u_\mu(n+1))^2$ , where  $u'(n+1)$  is the output of the network for the input  $u(n)$ .

These introduced fluctuations are necessary to compensate an unavoidable imperfection of the training and provide robustness for the trained neural network map. One can never train the network one hundred percent perfect, i.e., to make its outputs  $u'(n+1)$  exactly be equal to the desired one  $u_\mu(n+1)$ . When the neural network map (5) is trained on many trajectory cuts of a dynamical system with various parameter values, as it is done in our previous works<sup>22,23</sup>, the map is able to reproduce well the dynamics even in spite of not perfect training. Now we have only one trajectory corresponding to a single set of control parameter values. Training the map (5) without the random sampling of  $u(n)$  and setting  $u(n) = \mu(n)$  instead is found to result in a fragile reconstructed system. Its iterations are unable to follow the training trajectory when even a small perturbation is added to the initial point. However, the random sampling of  $u(n)$  from the full Gaussian distribution  $N(\mu(n), \sigma(n))$

also results in inappropriate reconstructed system that is unable to reproduce the modeled trajectory at all. The desired neural network map that models the system (1) well is obtained when  $u(n)$  are sampled from the truncated normal distribution  $N(\mu(n), \sigma(n))$  with truncation at  $0.1\sigma$ . This particular value is not the single best one. We checked truncations between  $0.01\sigma$  and  $\sigma$  and observed similarly good results in a sense that the resulting maps reproduced the modeled system.

The neural network map (5) admits a vector  $p$  that models control parameters of the original dynamical system. In papers<sup>22,23</sup> we trained the map (5) on trajectories that were sampled at various parameter values of the modeled system. These values were scaled to the interval  $[-1, 1]$  and accompanied the corresponding trajectory samples as training data. In the present work the source of the training data is a single trajectory of (1) so that none of the parameters is emphasized over the others. For this reason we consider  $p$  as a scalar, i.e.,  $D_p = 1$ , and when the neural network map is trained, the trajectory data are accompanied with a single value  $p = 0.5$ . This constant is an arbitrary chosen value within the working range  $[-1, 1]$ . The seemingly more natural value  $p = 0$  cannot be chosen because then the corresponding network weights would be zeroed out and no training would take place.

When the training is finished we consider the dynamics of the resulting neural network map (5) at various  $p$ . It is interesting to establish the correspondence between the regimes of the original system (1) and its reconstructed version (5) at various parameter values.

### V. DYNAMICS OF THE NEURAL NETWORK MAP

We use the neural networks as described in Secs. III and IV to reconstruct dynamics of the system (1) from a single scalar time series. We solve Eqs. (1) numerically at fixed parameter set when this system demonstrates bursting oscillations as in Fig. 1, then take a time series  $S(n) = S(t_0 + n\Delta t)$  for one period of bursting, and construct delay-coordinate embedding vectors  $R(n)$  with the excessively large dimension  $D_e = 32$ . First these vectors are employed to train the VAE, and then the state-space vectors  $u(n)$  of the reduced dimension  $D_u = 3$  are reconstructed from  $R(n)$  by the encoder part of the VAE. In turn, the obtained  $u(n)$  are used to train the neural network map (5). During the training, the trajectory data are accompanied by the parameter value  $p = 0.5$ . In this section we examine the regimes of the trained map (5) at various  $p$  and contrast them with the regimes of the initial system (1).

Figures. 9, 10, and 11 demonstrate dynamics of the neural network map (5) trained for the system (1) at  $V_S = -36$  and  $k = 0$ . The initial trajectory is shown in Fig. 6(c). The data reconstructed by the VAE encoder and are used for training the neural network map are shown in Fig. 6(d-f).



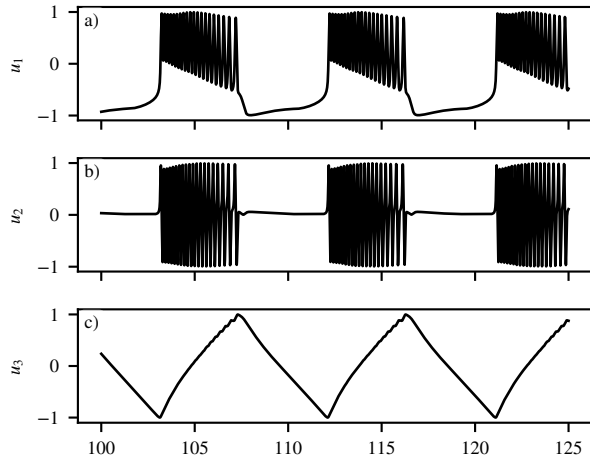


FIG. 9. Iteration of the neural network map (5) trained for the time series  $S(t)$  in Fig. 6(c). The parameter  $p$  equals to the training value  $p = 0.5$ . The starting point of the iterations is chosen arbitrarily.

Figure 9 is plotted at the point of training  $p = 0.5$ . Note that in this and in the following figures the starting point of the iterations is chosen at random, not from the training data. We see that the trajectory generated by the neural network map reproduces the training data very well, compare Fig. 9 and Fig. 6(d-f). As previously discussed, the VAE is unable to accurately reconstruct the precise structure of the variable  $n$  of the system (1), compare the original curve  $n(t)$  in Fig. 6(b) and its reconstructed version in Fig. 6(e). The neural network map accurately recovers this feature of the training data, compare Fig. 9(b) and 6(e).

It is of interest to observe the behavior of the map (5) when the value of  $p$  is taken beyond the training value. Figures 10 and 11 illustrate that varying  $p$  produces a comparable outcome to varying  $V_S$  in the system (1). As illustrated in Fig. 10 the system exhibits bursting at  $p = 0.8$ . Similarly, Fig. 11 reveals the presence of spikes at  $p = 0.2$ . These observations can be compared with Figs. 1 and 2, which show bursting and spiking in the system (1) at different values of  $V_S$ . Also it is important to note that spikes were not demonstrated to the neural network during training.

Figure 12 demonstrates the diagram of the regimes of the neural network map (5) trained for the system (1) at  $V_S = -36$  and  $k = 0$ . This figure is plotted in the same manner as Fig. 3. It is evident that the diagrams for the system (1) and its reconstructed model (5) exhibit a high degree of similarity. The most apparent and nonessential distinction is the directionality of the parameter variations. An increase in  $V_S$  is associated with a decrease in  $p$ .

It was observed that varying  $p$  is similar to varying  $V_S$  in the modeled system (1). However, this correspondence is not particularly noteworthy, as bursts and spikes are

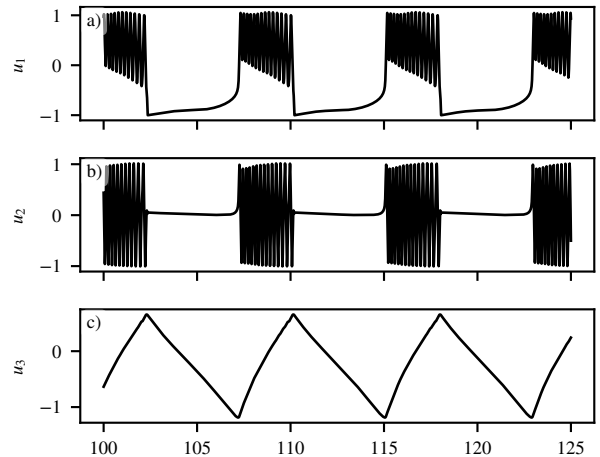


FIG. 10. Bursts produced as a result of iterations of the neural network map as in Fig. 9 for  $p$  beyond the training value,  $p = 0.8$ .

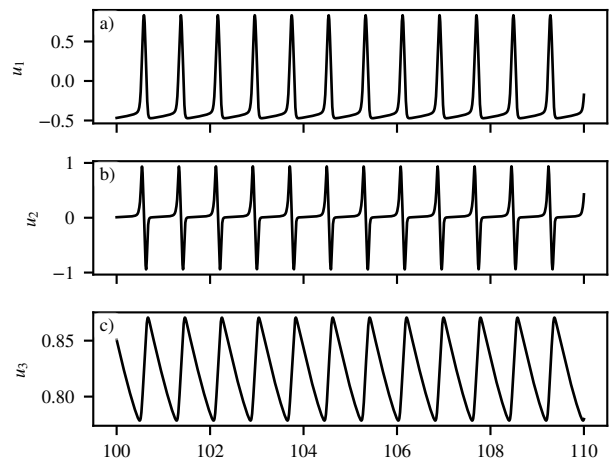


FIG. 11. Spiking in the neural network map as in Fig. 9 at  $p = 0.2$ .

the two most typical regimes of the system, and varying other parameters will also result in oscillations of these two types.

The system (1) exhibits a single fixed point that within the considered parameter range is always unstable at  $k = 0$ . The modification at  $k = 1$  results in the area where the fixed point becomes stable, thereby initiating bistability between the bursting and the fixed point. In our previous work<sup>22</sup> we demonstrated that the neural network map (5) can discover the fixed point. To train the map we used various trajectory cuts of the system (1) that never approached the fixed point. The trained neural network map as expected was able to reproduce the bursting and spiking dynamics, because this behavior were shown it in the course of training. But also the map discovered the fixed point with its correct

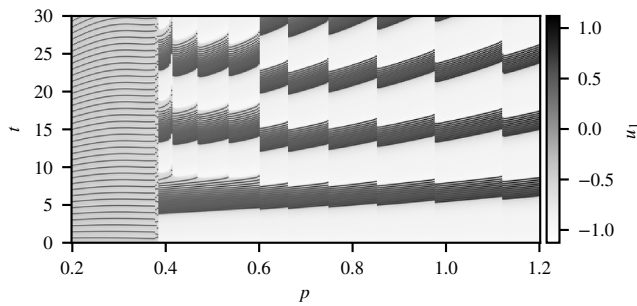


FIG. 12. Diagrams of regimes of the neural network map (5) trained for the system (1) at  $V_S = -36$  and  $k = 0$ . The parameter  $p$  is represented horizontally, with the vertical axis corresponding to time. Gray shades indicate values of the variable  $u_1$ , which reproduces the variable  $V$  of the system (1). Compare it with the diagram in Fig. 3.

stability properties, see Fig. 8 of the referred paper<sup>22</sup>. In the present paper, we consider a more complex situation. The only information about the system is one period of its bursting trajectory, which is displayed to the neural network map via the single variable  $S$ . We train this network and aim to ascertain which properties of the fixed point can be recovered by the network in this case.

Due to the fact that no fixed point information is explicitly presented to the neural network during the training process, the resulting neural network map usually has more than one fixed point. Some of these fixed points are located at a considerable distance from the origin and thus they are not considered because the bursting and spiking oscillations occur within the range  $u_i \in [-1, 1]$  as a result of the preliminary rescaling of the training data. Moreover, the distinct training runs may yield disparate sets of fixed points due to the random initialization of the network weights. To identify nevertheless patterns in the fixed points appearance for each parameter of the system (1), we will train three neural network maps that differ only in their initial random weights. Thus, the parameter values of the system (1) will be considered in eight combinations:  $V_S = -35.5, -36, -36.5$  and  $-38$  at  $k = 0$  and  $k = 1$ , for each parameter set the time series of  $S(t)$  will be computed, the VAE will be trained on it, and then three versions of the neural network map will be trained for each dataset produced by the VAE encoder.

To illustrate the results, we plot the distance of the fixed point from the origin, denoted by  $\rho$ , as a function of  $p$  in the vicinity of the training value  $p = 0.5$ , see Fig. 13. Stable and unstable fixed points are shown with black and orange colors, respectively, and additionally marked by the symbols “-” and “+” in the legends. The three versions of the neural network map are shown with markers of different shapes.

As one can see in Fig. 4, the parameters  $V_S = -35.5, -36$ , and  $-36.5$  lay within the area of bistability when  $k = 1$ , while at  $k = 0$  the fixed point is always unstable, Fig. 3. The fixed points of the neural network maps (5) reconstructed for these parameter values at  $k = 0$  are

shown in Figs. 13(a, b, c). It is noteworthy that there are no stable fixed points at  $p = 0.5$  and in the vicinity of this value, which is consistent with the properties of the system (1) at  $k = 0$ . Figures 13(e, f, g) corresponds to the maps trained when the modeled system had a stable fixed point at  $k = 1$ . One sees that at  $V_S = -35.5$  and  $-36$ , Figs. 13(e, f), respectively, all three reconstructed maps also have a stable fixed point. However, for the maps trained at  $V_S = -36.5$ , Fig. 13(g), only one of them exhibits the expected stable fixed point, while for two others the fixed point is unstable even exactly at the training point  $p = 0.5$ .

Regardless of  $k$ , the fixed point of the modeled system (1) is unstable at  $V_S = -38$ . Consequently, all reconstructed maps also lack stable fixed points at  $p = 0.5$  and in the vicinity of this value, see Figs. 13(d, h).

In conclusion, the training procedures under discussion do not consistently recovers the stability property of the fixed point of the system (1). However, a clear trend has been observed: in the presented examples, only one of eight considered cases does not fully correspond to the expected behavior: in Fig. 13(g) not all runs of the training result in the expected stable fixed point.

When the system (1) is reconstructed at parameter values where its fixed point is stable, say  $k = 1$ ,  $V_S = -36$ , and the trained map correctly identifies the stability property of this point, a diagram of regimes with bistability similar to that in Fig. 4 can be plotted, see Fig. 14. In Fig. 14(a) we compute a solution starting from an arbitrary initial point at  $p = 0.5$  and then continue this solution to the left and to the right. Then we find the stable fixed point at  $p = 0.5$  and again continue it to the left and to the right, Fig. 14(b). It can be observed that the fixed point remains stable approximately for  $p \in [0.4, 1]$ , while outside of this range, the oscillating solutions, burst and spikes, appear. It is notable that this diagram is sufficiently similar to the diagram plotted directly for the system 1, see Fig. 4.

## VI. CONCLUSION

This work examines the reconstruction using neural networks of a family of dynamical systems with neuro-morphic behavior from a single scalar time series. We consider a model of a physiological neuron built on the basis of the Hodgkin-Huxley formalism. Taking its single scalar time series at fixed values of the control parameters, we reconstruct a one-parameter family of dynamical systems as a neural network map and study the correspondence of the behavior of this family to the behavior of the Hodgkin-Huxley neuron for various parameter values.

The general motivation of this work is a contribution to a theoretical framework for processing experimental data. A typical situation when working with experimental data is that there is a single record of an experiment from which it is necessary to extract the maximum amount of

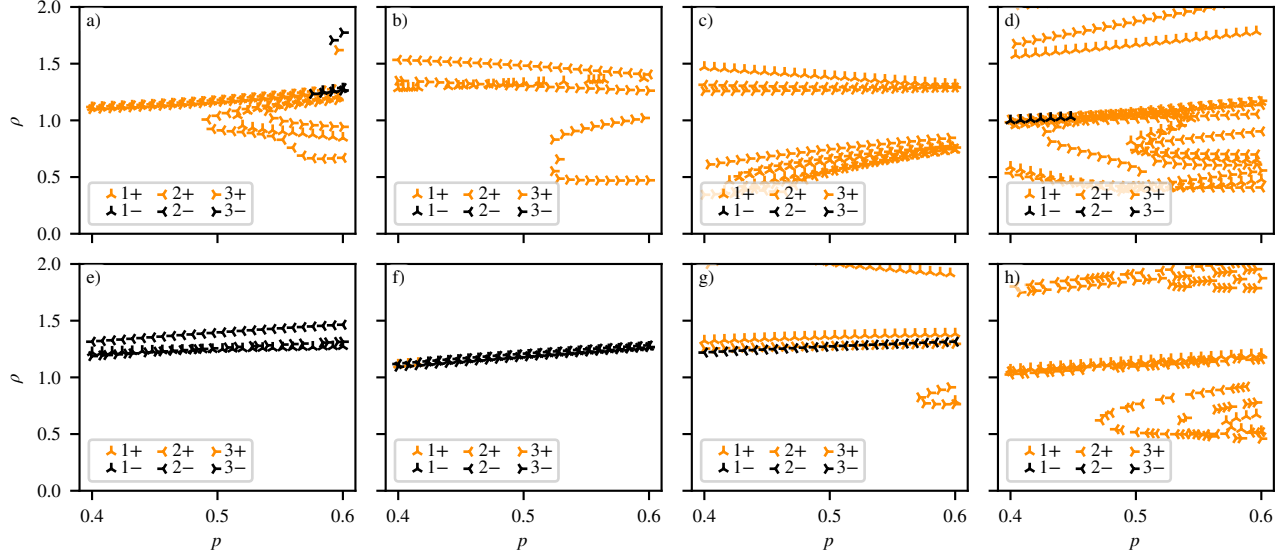


FIG. 13. Distance  $\rho$  to the origin of fixed points of neural network maps (5) trained for different parameters  $k$  and  $V_S$  of the system (1). Along the horizontal axes are plotted the values of the parameter  $p$ . Panels (a–d) in the upper row correspond to the case  $k = 0$  and for panels (e–h) in the lower row  $k = 1$ . Columns of panels from left to right demonstrate variation of  $V_S$ : (a) and (e)  $V_S = -35.5$ ; (b) and (f)  $V_S = -36$ ; (c) and (g)  $V_S = -36.5$ ; (d) and (h)  $V_S = -38$ . Each panel contains three curves corresponding to three neural network maps trained for identical parameters and random initial network weights. The curves are plotted with triangle markers 1, 2 and 3. Black and orange colors of the markers indicate stability of the corresponding fixed point. Black color with “–” in the legends indicate stable fixed point, and orange marker with “+” depict unstable fixed points.

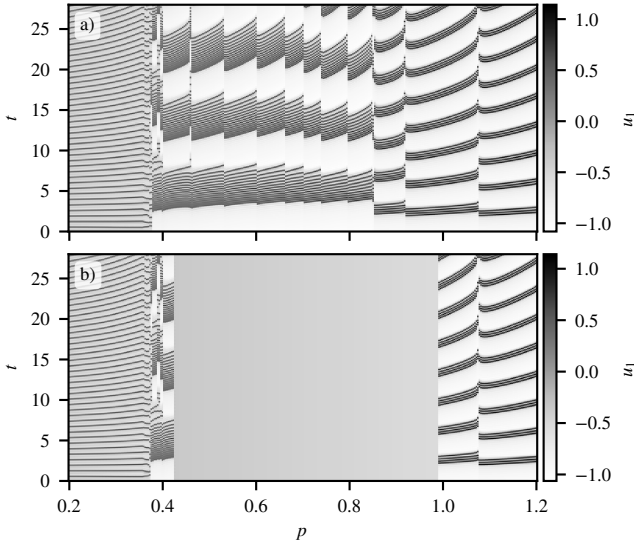


FIG. 14. Diagram of regimes of the neural network map (5) trained for the system (1) at  $V_S = -36$  and  $k = 1$ . Panels (a) and (b) are computed as continuations of two solutions, the bursting and the fixed point, respectively, computed in the middle part of figure at  $p = 0.5$ .

information about the full-scale system under the study. In this work, we simulate such a situation, but for now we do not set a goal to reproduce it exactly, namely: our

time series is obtained as a result of solving a system of differential equations, the data is recorded with a sufficiently small time step and is not noisy.

The reconstructed family of dynamical systems is a neural network, which after the training operates as a recurrent map, i.e., a discrete-time dynamical system, and has one control parameter. The reconstruction is performed for a scalar time series of the original system in bursting mode.

It is shown that, despite the fact that the spiking oscillations are not demonstrated to the network during training, the reconstructed neural network map, when changing the parameter, demonstrates the transition from bursts to spikes in a qualitatively similar way to how it occurs in the modeled system. For the modeled system and the neural network map, diagrams or regimes are represented that show the transition from bursts to spikes. The diagrams correspond well to each other.

The situation is studied when a modification is introduced into the Hodgkin-Huxley system, which makes it possible for the emergence of a bistability regime of burst dynamics and a stable fixed point. The neural network map was reconstructed from the bursting trajectory of such a system in the bistability mode, and it was shown that it can also have a stable fixed point. The represented diagrams of regimes for bistability demonstrate qualitative agreement with similar diagrams of the simulated system.

The stability of fixed points of neural network map

reconstructed for different values of the parameters of the modeled system in the presence and absence of a modification that generates bistability is studied. Note that during the training process the fixed point was never demonstrated to the neural network. It is shown that the nature of the stability of fixed points present in the neural network maps trained in this way does not always strictly correspond to the system being modeled. However, by performing the training procedure several times for the same parameters of the modeled system, we showed that there is a clearly visible tendency towards a much more frequent appearance of fixed points with the “correct” character of stability.

When reconstructing a dynamical system from a scalar time series, the question arises about the dimension of the reconstructed state-space vectors. In our work, we construct for a time series delay-coordinate embedding vectors, while setting their dimension to be excessively large, namely ten times larger than the true dimension of the state-space vectors of the modeled system. Then their dimension is reduced using a variational autoencoder, which in its latent space restores the system state vectors. These vectors are subsequently used for training the neural network map. The question of the correct choice of the dimension of the reconstructed state-space vectors is discussed. It is shown that the true dimension corresponding to the dimension of the modeled system can be found on the basis of varying the dimension of the latent space and analyzing the patterns in the appearance of new components, as well as by observing the changes in the behavior of learning curves.

## ACKNOWLEDGMENTS

This work was supported by the Russian Science Foundation, 20-71-10048, <https://rscf.ru/en/project/20-71-10048/>. The study of model dynamics was carried out within the framework of the project “Mirror Laboratories” HSE University (Section II).

## DATA AVAILABILITY STATEMENT

The data that support the findings of this study are available within the article.

## Appendix A: Functions and parameter values of the Hodgkin-Huxley-type model

The functions included to Eqs. (1) are as follows:

$$I_{Ca}(V) = g_{Ca} m_{\infty}(V) (V - V_{Ca}), \quad (\text{A1a})$$

$$I_K(V, n) = g_K n (V - V_K), \quad (\text{A1b})$$

$$I_S(V, S) = g_S S (V - V_K), \quad (\text{A1c})$$

$$I_{K2}(V) = g_{K2} p_{\infty}(V) (V - V_K), \quad (\text{A1d})$$

$$\omega_{\infty}(V) = \left( 1 + \exp \frac{V_{\infty} - V}{\theta_{\omega}} \right)^{-1}, \quad \omega = m, n, S, \quad (\text{A1e})$$

$$p_{\infty}(V) = \left( \exp \frac{V - V_p}{\theta_p} + \exp \frac{V_p - V}{\theta_p} \right)^{-1}. \quad (\text{A1f})$$

Numerical values of the control parameters used in simulations of the system (1) can be found in Table I.

TABLE I. Numerical values of parameters of the model (1)

$\tau = 0.02 \text{ s}$	$\tau_S = 35 \text{ s}$	$\sigma = 0.93$	
$g_{Ca} = 3.6$	$g_K = 10$	$g_S = 4$	$g_{K2} = 0.12$
$V_{Ca} = 25 \text{ mV}$	$V_K = -75 \text{ mV}$		
$\theta_m = 12 \text{ mV}$	$\theta_n = 5.6 \text{ mV}$	$\theta_S = 10 \text{ mV}$	$\theta_p = 1 \text{ mV}$
$V_m = -20 \text{ mV}$	$V_n = -16 \text{ mV}$	$V_S = -36 \text{ mV}$	$V_p = -49.5 \text{ mV}$

## Appendix B: Structure of VAE in detail

The VAE we create for our problem is shown in Fig. 15. Figure 15(a) demonstrates its common structure and in Figs. 15(b, c) the inner structures of the encoder and decoder are shown.

The input vector  $R$  is forwarded to the encoder that maps it to a couple of vectors  $\mu, \nu \in \mathbb{R}^{D_u}$ . Their dimension  $D_u < D_e$  is the dimension of the reconstructed dynamical system. The vector  $\nu$  is treated as a logarithm of a variance, and  $\sigma = e^{\nu/2}$  is a standard deviation. The vectors  $\mu$  and  $\sigma$  defines so called a latent space. Elements of this space are vectors  $u$  that represent the reduced form of  $R$ . Vectors  $u$  from the latent space are taken as a random samples of a normal distribution  $N(\mu, \sigma)$ . So, when  $\mu$  and  $\sigma$  are generated for the input  $R$  the vector  $u$  is sampled and then sent to the decoder. It maps this vector to  $R'$ . The goal of VAE training is minimization of the discrepancy between  $R$  and  $R'$  by tuning parameter vectors of the encoder  $w_e$  and the decoder  $w_d$ . Also a proper latent space structure has to be provided that is achieved by simultaneous minimization of the Kullback–Leibler divergence between the distribution parameterized by  $\mu$  and  $\sigma$  and standard normal distribution<sup>20</sup>. Thus the loss function for VAE training includes two terms<sup>21</sup>: the discrepancy between  $R$  and  $R'$  that we compute as a mean squared error and

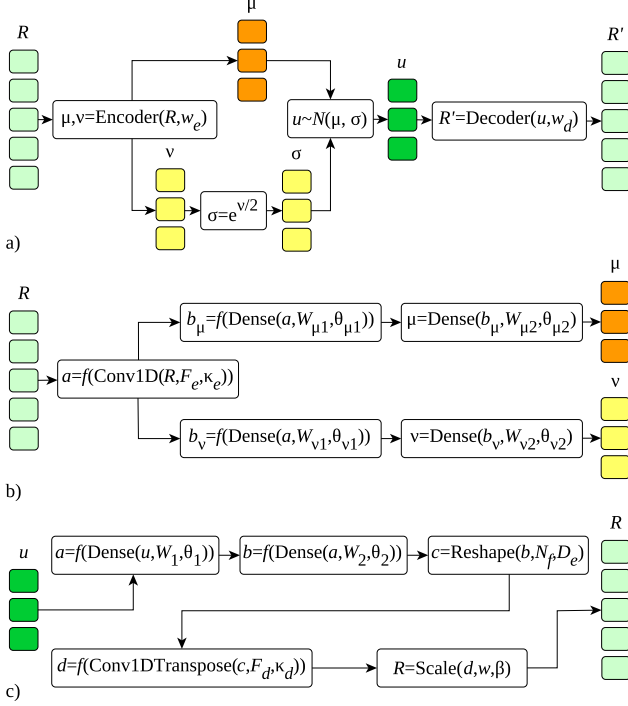


FIG. 15. VAE: (a) general structure; (b) and (c) inner structure of the encoder and decoder, respectively.  $R$  is the input vector;  $\mu$  and  $\sigma$  are parameters of the latent space;  $u$  is a vector of the latent space sampled from the Gaussian distribution  $N(\mu, \sigma)$ ;  $R'$  is the output vector;  $w_e$  and  $w_d$  are vectors of trainable parameters (neural networks weights) of the encoder and the decoder respectively:  $w_e = \{F_e, \kappa_e, W_{\mu 1, 2}, \theta_{\mu 1, 2}, W_{\nu 1, 2}, \theta_{\nu 1, 2}\}$ ,  $w_d = \{W_{1, 2}, \theta_{1, 2}, F_d, \kappa_d, w, \beta\}$ .

the mean Kullback–Leibler divergence computed via  $\mu$  and  $\nu$ :

$$L = \langle \langle (R - R')^2 \rangle \rangle_{D_e} + K \langle \mu^2 + e^\nu - \nu - 1 \rangle_{D_u} \quad (\text{B1})$$

The first and the second terms are averaged over  $D_e$  and  $D_u$  components of the corresponding vectors, respectively. The coefficient  $K$  is introduced to balance minimization rates of the two terms: one sees that the first one can be arbitrary small while the second one is at least  $O(1)$ . Thus the value of  $K$  has to be of the order of the acceptable recovery error. We are going to continue the training until the mean squared recovery error is of the order  $10^{-5}$ . Thus we set  $K = 10^{-5}$ .

The common architecture of VAE displayed in Fig. 15(a) is typical for various topics, while the inner structures of the encoder and decoder depend on the problem under consideration. In our case time series are processed. There are three standard ways for dealing with them: one dimensional convolutions, recurrent cells and transformers<sup>21</sup>. Since we aim to keep our neural networks as simple as possible, the convolutions are employed. The encoder includes one convolution layer supplied with two dense layers, Fig. 15(b). The decoder

TABLE II. Structure of elements of the encoder and the decoder in Figs 15(b,c).  $N_k$  is convolution kernel size,  $N_f$  is number of convolution filters,  $N_{\mu 1}$  is size of the output of the first dense layer.  $N_k = 3$ ,  $N_f = 16$ .  $N_{\mu 1} = 512$ ,  $f(\cdot) = \tanh(\cdot)$ .

Object	Type	Diemsnion
$R$	row vector	$D_e$
$F_e, F_d$	matrix	$N_k \times N_f$
$\kappa_e$	row vector	$N_f$
$\kappa_d$	scalar	
$W_{\mu 1}, W_{\sigma 1}$	matrix	$(D_e N_f) \times N_{\mu 1}$
$\theta_{\mu 1}, \theta_{\sigma 1}$	row vector	$N_{\mu 1}$
$W_{\mu 2}, W_{\sigma 2}$	matrix	$N_{\mu 1} \times D_u$
$\theta_{\mu 2}, \theta_{\sigma 2}$	row vector	$D_u$
$W_1$	matrix	$D_u \times N_{\mu 1}$
$\theta_1$	row vector	$N_{\mu 1}$
$W_2$	matrix	$N_{\mu 1} \times (D_e N_f)$
$\theta_2$	row vector	$D_e N_f$
$w, \beta$	scalars	
$f(\cdot)$	scalar function of scalar argument	

TABLE III. Structure of elements of Eq. (5). For models in this paper  $D_u = 3$ ,  $D_p = 1$ ,  $N_h = 100$ ,  $f(\cdot) = g(\cdot) = \tanh(\cdot)$ , and  $\chi = \Delta t = 0.005$ .

Object	Type	Diemsnion
$u(n)$	row vector	$D_u$
$u_i(n)$	scalar	
$u_{-i}(n)$	row vector	$D_u - 1$
$p$	row vector	$D_p$
$a_i, \mu_i$ and $\beta_i$	row vectors	$N_h$
$b_i$	column vector	$N_h$
$\gamma_i$	scalar	
$A_i$	matrix	$(D_u - 1) \times N_h$
$B_i$	matrix	$D_p \times N_h$
$f(\cdot)$ and $g(\cdot)$	scalar functions of scalar argument	
$\chi$	small scalar constant	

have to perform the encoder operation in the reversed order. Thus it first includes two dense layers. Then the flat output of these layers is reshaped to the matrix  $N_f \times D_e$  to fulfill the requirement for the input data of the transposed convolution layer. Its output is one dimensional vector  $d$  that is scaled as  $R = \text{Scale}(d, w, \beta) = dw + \beta$  with scalar trainable coefficients  $w$  and  $\beta$  to fit the range of the desired output vector  $R$ . Table II provides the description of the elements of the encoder and decoder. See also the book<sup>21</sup> for more descriptions of the layers used.

### Appendix C: Detail of the neural network map

Structure of Eq. (5) corresponds to a two-layer dense network. The first layer obtains a scalar value  $u_i$  and its output is a vector of dimension  $N_h$  that is the result of the expression  $f(u_i(n)a_i + \mu_i + g(\dots))$ . Layers like this are usually called hidden. Its dimension  $N_h$  determines a network information capacity and performance. Unlike a generic two-layer network, the vector of biases  $\mu_i$  get a correction form the output of an additional layer  $g(u_{\neg i}(n)A_i + pB_i + \beta_i)$  that depends on other (non  $i$ th) dynamical variables and control parameters. The second layer, i.e., network output has a form  $f(\dots)b_i + \gamma_i$ . It computes a scalar value that is used as a correction to  $u_i(n)$  to compute its value on step  $n + 1$ :  $u_i(n + 1) = u_i(n) + \chi(\dots)$ .

The neural network map (5) is adopted for a required dynamics during training procedure that consists of tuning the network weight parameters

$$w_m = \{a_i, \mu_i, A_i, B_i, \beta_i, b_i, \gamma_i \mid i = 1, 2, \dots, D_u\}. \quad (\text{C1})$$

The training vector  $u(n)$  is forwarded to the network and the network computes  $u'(n + 1)$ . This vector is compared with the desired one  $u(n + 1)$ . Their mean squared error is a loss function of the training process. It is minimized in course of training via gradient decent method<sup>21</sup>. In actual computations we used the modification of this method named Adam<sup>39</sup>. When training is finished and the network operates as a discrete time dynamical system, we set  $u'(n + 1) = u(n + 1)$ .

Software implementation of the neural network map (5) can be done via the following operators. Operator  $\text{Take}(u, i)$  extracts  $i$ th elements of the vector  $u$  and  $\text{Sans}(u, i)$  removes it and returns a vector  $u_{\neg i}$  without this element. Operator  $\text{Dense}(x, W, b) = xW + b$  represents a fully connected (dense) layer without the activation: input row vector  $x$  is multiplied by a matrix  $W$  and biased by a vector  $b$ . Finally, square brackets  $[\cdot, \cdot]$  denotes concatenation of two vectors or matrices.

In this notation neural network map (5) for  $i$ th components can be described as follows, see Fig. 16 and Eqs. (C2). There are two input vectors,  $u$  and  $p$ , Eq. (C2a). Vector  $u$  is split into a scalar  $u_i$  and a vector  $u_{\neg i}$  without the  $i$ th element, Eqs. (C2b). Layer in Eq. (C2c) takes  $u_{\neg i}$  and  $p$  and compute a vector  $h_i$  of dimension  $N_h$ . This vector carries an information about the influence from the control parameters  $p$  and all elements of  $u$  except the  $i$ th. This vector is added to the output of the layer that processes the  $i$ th component (C2d). At the output of this layer the vector  $q_i$  appears that has the dimension  $N_h$ . It is passed to the last layer in Eq. (C2e) whose output is used to compute the solution at the new time step  $v'_i$ . Doing these computations for  $i = 1, 2, \dots, D_u$  we obtain the full vector at next time

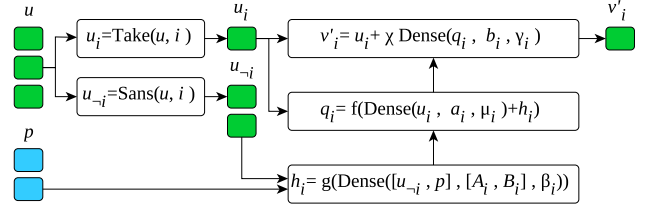


FIG. 16. Structure of the neural network for the  $i$ th variable of the map (5). Here  $u \equiv u(n)$ ,  $v'_i \equiv u'_i(n + 1)$ . The prime marks a resulting value computed by the network. This value in the course of training is compared with the “correct” value  $u_i(n + 1)$  from the training dataset.

step  $v' = u'(n + 1)$ .

$$p = \text{Input}(), \quad u = \text{Input}(), \quad (\text{C2a})$$

$$u_i = \text{Take}(u, i), \quad u_{\neg i} = \text{Sans}(u, i), \quad (\text{C2b})$$

$$h_i = g(\text{Dense}([u_{\neg i}, p], [A_i, B_i], \beta_i)), \quad (\text{C2c})$$

$$q_i = f(\text{Dense}(u_i, a_i, \mu_i) + h_i), \quad (\text{C2d})$$

$$v'_i = u_i + \chi \text{Dense}(q_i, b_i, \gamma_i). \quad (\text{C2e})$$

As already mentioned above, the computed output  $u'(n + 1)$  is compared with the desired one  $u(n + 1)$  during training, and when the training is finished we set  $u'(n + 1) = u(n + 1)$ .

- <sup>1</sup>H. Kantz and T. Schreiber, *Nonlinear time series analysis*, 2nd ed. (Cambridge University Press, Cambridge, UK, 2004) p. 388.
- <sup>2</sup>E. Bradley and H. Kantz, “Nonlinear time-series analysis revisited,” *Chaos: An Interdisciplinary Journal of Nonlinear Science* **25**, 097610 (2015).
- <sup>3</sup>B. P. Bezruchko and D. A. Smirnov, *Extracting knowledge from time series*, edited by D. A. Smirnov, Springer Series in Synergetics (Springer Science & Business Media, Berlin, Heidelberg, 2010) p. 410.
- <sup>4</sup>J. J. Scully, A. B. Neiman, and A. L. Shilnikov, “Measuring chaos in the Lorenz and Rössler models: Fidelity tests for reservoir computing,” *Chaos: An Interdisciplinary Journal of Nonlinear Science* **31**, 093121 (2021).
- <sup>5</sup>L.-W. Kong, H.-W. Fan, C. Grebogi, and Y.-C. Lai, “Machine learning prediction of critical transition and system collapse,” *Phys. Rev. Res.* **3**, 013090 (2021).
- <sup>6</sup>J. D. Hart, “Attractor reconstruction with reservoir computers: The effect of the reservoir’s conditional Lyapunov exponents on faithful attractor reconstruction,” *Chaos: An Interdisciplinary Journal of Nonlinear Science* **34**, 043123 (2024).
- <sup>7</sup>A. Flynn, V. A. Tsachouridis, and A. Amann, “Multifunctionality in a reservoir computer,” *Chaos: An Interdisciplinary Journal of Nonlinear Science* **31**, 013125 (2021).
- <sup>8</sup>A. Flynn, V. A. Tsachouridis, and A. Amann, “Seeing double with a multifunctional reservoir computer,” *Chaos: An Interdisciplinary Journal of Nonlinear Science* **33**, 113115 (2023).
- <sup>9</sup>D. Durstewitz, G. Koppe, and M. I. Thurm, “Reconstructing computational system dynamics from neural data with recurrent neural networks,” *Nature Reviews Neuroscience* **24**, 693–710 (2023).
- <sup>10</sup>Z. Zhang, Y. Zhao, J. Liu, S. Wang, R. Tao, R. Xin, and J. Zhang, “A general deep learning framework for network reconstruction and dynamics learning,” *Applied Network Science* **4**, 110 (2019).
- <sup>11</sup>N. Almazova, G. D. Barmparis, and G. P. Tsironis, “Analysis of chaotic dynamical systems with autoencoders,” *Chaos* **31**, 103109 (2021).

- <sup>12</sup>Y. Wu, Q. Ding, W. Huang, T. Li, D. Yu, and Y. Jia, “Dynamic learning of synchronization in coupled nonlinear systems,” *Nonlinear Dynamics* **112**, 21945–21967 (2024).
- <sup>13</sup>Z. Ye, Y. Wu, Q. Ding, Y. Xie, and Y. Jia, “Finding synchronization state of higher-order motif networks by dynamic learning,” *Phys. Rev. Res.* **6**, 033071 (2024).
- <sup>14</sup>Y. Wu, Q. Ding, W. Huang, X. Hu, Z. Ye, and Y. Jia, “Dynamic modulation of external excitation enhance synchronization in complex neuronal network,” *Chaos, Solitons & Fractals* **183**, 114896 (2024).
- <sup>15</sup>Y. Wu, W. Huang, Q. Ding, Y. Jia, L. Yang, and Z. Fu, “Enhancing orderly signal propagation between layers of neuronal networks through spike timing-dependent plasticity,” *Physics Letters A* **519**, 129721 (2024).
- <sup>16</sup>E. Levin, R. Gewirtzman, and G. F. Inbar, “Neural network architecture for adaptive system modeling and control,” *Neural Networks* **4**, 185–191 (1991).
- <sup>17</sup>B. Grieger and M. Latif, “Reconstruction of the El Niño attractor with neural networks,” *Climate Dynamics* **10**, 267–276 (1994).
- <sup>18</sup>H. G. Zimmermann and R. Neuneier, *Combining state space reconstruction and forecasting by neural networks*, edited by G. Bol, G. Nakhaeizadeh, and K.-H. Vollmer (Physica-Verlag HD, 2000) pp. 259–267.
- <sup>19</sup>W. Gilpin, Y. Huang, and D. B. Forger, “Learning dynamics from large biological data sets: Machine learning meets systems biology,” *Current Opinion in Systems Biology* **22**, 1–7 (2020).
- <sup>20</sup>D. P. Kingma and M. Welling, “An introduction to variational autoencoders,” *Foundations and Trends® in Machine Learning* **12**, 307–392 (2019).
- <sup>21</sup>F. Chollet, *Deep learning with Python*, 2nd ed. (Simon and Schuster, Shelter Island, NY, 2021) p. 504.
- <sup>22</sup>P. V. Kuptsov, N. V. Stankevich, and E. R. Bagautdinova, “Discovering dynamical features of Hodgkin-Huxley-type model of physiological neuron using artificial neural network,” *Chaos, Solitons & Fractals* **167**, 113027 (2023).
- <sup>23</sup>P. V. Kuptsov and N. V. Stankevich, “Modeling of the Hodgkin–Huxley neural oscillators dynamics using an artificial neural network (in russian),” *Izvestiya VUZ. Applied Nonlinear Dynamics* **32**, 72–95 (2024).
- <sup>24</sup>A. N. Kolmogorov, “On the representation of continuous functions of several variables by superpositions of continuous functions of a smaller number of variables,” *Doklady Akademii Nauk SSSR* **108**, 179–182 (1956), english translation: *Amer. Math. Soc. Transl.*, 17 (1961), pp. 369–373.
- <sup>25</sup>V. I. Arnold, “On functions of three variables,” *Doklady Akademii Nauk SSSR* **114**, 679–681 (1957), english translation: *Amer. Math. Soc. Transl.*, 28 (1963), pp. 51–54.
- <sup>26</sup>A. N. Kolmogorov, “On the representation of continuous functions of many variables by superposition of continuous functions of one variable and addition,” *Doklady Akademii Nauk SSSR* **114**, 953–956 (1957), english translation: *Amer. Math. Soc. Transl.*, 28 (1963), pp. 55–59.
- <sup>27</sup>G. Cybenko, “Approximation by superpositions of a sigmoidal function,” *Mathematics of Control, Signals and Systems* **2**, 303–314 (1989).
- <sup>28</sup>A. N. Gorban, “Generalized approximation theorem and exact representation of polynomials in multiple variables via superpositions of polynomials in one variable (in Russian),” *Izvestiya VUZ. Mathematics* **432**, 6–9 (1998).
- <sup>29</sup>S. Haykin, *Neural networks: a comprehensive foundation*, 2nd ed. (Prentice Hall, Upper Saddle River, NJ, 1998) p. 842.
- <sup>30</sup>P. V. Kuptsov, A. V. Kuptsova, and N. V. Stankevich, “Artificial neural network as a universal model of nonlinear dynamical systems,” *Russian Journal of Nonlinear Dynamics* **17**, 5–21 (2021).
- <sup>31</sup>A. Sherman, J. Rinzel, and J. Keizer, “Emergence of organized bursting in clusters of pancreatic beta-cells by channel sharing,” *Biophysical Journal* **54**, 411–425 (1988).
- <sup>32</sup>N. Stankevich and E. Mosekilde, “Coexistence between silent and bursting states in a biophysical Hodgkin-Huxley-type of model,” *Chaos: An Interdisciplinary Journal of Nonlinear Science* **27**, 123101 (2017).
- <sup>33</sup>E. Hairer and G. Wanner, “Stiff differential equations solved by radau methods,” *Journal of Computational and Applied Mathematics* **111**, 93–111 (1999).
- <sup>34</sup>A. Shilnikov and G. Cymbalyuk, “Transition between tonic spiking and bursting in a neuron model via the blue-sky catastrophe,” *Phys. Rev. Lett.* **94**, 048101 (2005).
- <sup>35</sup>P. V. Kuptsov and A. V. Kuptsova, “Estimating of the inertial manifold dimension for a chaotic attractor of complex Ginzburg-Landau equation using a neural network,” *Proc. of SPIE* **11067**, 110670N–1 (2019).
- <sup>36</sup>N. H. Packard, J. P. Crutchfield, J. D. Farmer, and R. S. Shaw, “Geometry from a time series,” *Phys. Rev. Lett.* **45**, 712–716 (1980).
- <sup>37</sup>F. Takens, “*Dynamical Systems and Turbulence*,” (Springer, Berlin, 1981) Chap. Detecting strange attractors in fluid turbulence, pp. 366–381.
- <sup>38</sup>W. H. Press, S. A. Teukolsky, W. T. Vetterling, and B. P. Flannery, *Numerical recipes*, 3rd ed., edited by W. H. Press (Cambridge University Press, Cambridge [u.a.], 2007).
- <sup>39</sup>D. P. Kingma and J. Ba, “Adam: A method for stochastic optimization,” *arXiv:1412.6980 [cs.LG]* (2014), published as a conference paper at International Conference on Learning Representations (ICLR) 2015, *arXiv:1412.6980 [cs.LG]*.